Quantifying the cerebral metabolic rate of oxygen by combining diffuse correlation spectroscopy and time-resolved near-infrared spectroscopy

Kyle Verdecchia
Mamadou Diop
Ting-Yim Lee
Keith St. Lawrence

Quantifying the cerebral metabolic rate of oxygen by combining diffuse correlation spectroscopy and time-resolved near-infrared spectroscopy

Kyle Verdecchia,[a,b] **Mamadou Diop,**[a,b] **Ting-Yim Lee,**[a,b,c] **and Keith St. Lawrence**[a,b]
[a]Lawson Health Research Institute, Imaging Division, London, Ontario, N6A 4V2, Canada
[b]Western University, Department of Medical Biophysics, London, Ontario, N6A 5C1, Canada
[c]Robarts Research Institute, Imaging Program, 100 Perth Drive, London, Ontario, N6A 5K8, Canada

Abstract. Preterm infants are highly susceptible to ischemic brain injury; consequently, continuous bedside monitoring to detect ischemia before irreversible damage occurs would improve patient outcome. In addition to monitoring cerebral blood flow (CBF), assessing the cerebral metabolic rate of oxygen ($CMRO_2$) would be beneficial considering that metabolic thresholds can be used to evaluate tissue viability. The purpose of this study was to demonstrate that changes in absolute $CMRO_2$ could be measured by combining diffuse correlation spectroscopy (DCS) with time-resolved near-infrared spectroscopy (TR-NIRS). Absolute CBF was determined using bolus-tracking TR-NIRS to calibrate the DCS measurements. Cerebral venous blood oxygenation (SvO_2) was determined by multiwavelength TR-NIRS measurements, the accuracy of which was assessed by directly measuring the oxygenation of sagittal sinus blood. In eight newborn piglets, $CMRO_2$ was manipulated by varying the anesthetics and by injecting sodium cyanide. No significant differences were found between the two sets of SvO_2 measurements obtained by TR-NIRS or sagittal sinus blood samples and the corresponding $CMRO_2$ measurements. Bland–Altman analysis showed a mean $CMRO_2$ difference of 0.0268 ± 0.8340 mL $O_2/100$ g/ min between the two techniques over a range from 0.3 to 4 mL $O_2/100$ g/ min. © *2013 Society of Photo-Optical Instrumentation Engineers (SPIE)* [DOI: 10.1117/1.JBO.18.2.027007]

Keywords: diffuse correlation spectroscopy; time-resolved near-infrared spectroscopy; cerebral metabolic rate of oxygen; cerebral blood flow; newborn piglet; premature neonates.

Paper 12611 received Sep. 14, 2012; revised manuscript received Jan. 11, 2013; accepted for publication Jan. 14, 2013; published online Feb. 6, 2013.

1 Introduction

Improvements in neonatal intensive care have reduced the mortality rate associated with preterm birth, but unfortunately these infants remain at a high risk of neurological complications, including learning disabilities and cerebral palsy.[1] Preterm infants are vulnerable to ischemic and hemorrhagic brain injury in part because of an underdeveloped cerebral vasculature, including limited or impaired autoregulation.[2] As a result, unstable arterial blood pressure could lead to dangerous fluctuations in cerebral blood flow (CBF). Recent studies using near-infrared spectroscopy (NIRS) to monitor cerebral blood oxygenation have reported that periods of impaired autoregulation are not uncommon in preterm infants; however, a correlation between the occurrence of impaired autoregulations and brain lesions was not observed.[3–5]

Using cerebral blood oxygenation to identify critical CBF thresholds is potentially confounded by the indirect relationship between cerebral blood oxygenation and CBF, as the former also depends on the cerebral metabolic rate of oxygen ($CMRO_2$), the cerebral blood volume (CBV), and arterial oxygen saturation.[6] An alternative approach would be to combine NIRS with diffuse correlation spectroscopy (DCS), an emerging optical method sensitive to CBF.[7–9] This combination has the advantage of providing a means of monitoring both CBF and $CMRO_2$.[10–12] The latter can be determined from blood oxygenation and flow measurements and is considered a more sensitive indicator of tissue viability.[13,14] For example, $CMRO_2$ has been shown to be more sensitive to the severity of cerebral hypoxia-ischemia than NIRS oxygenation measurements alone.[15,16] The combination of NIRS and DCS could therefore help identify clinically significant passive-pressure CBF by detecting flow fluctuations large enough to affect cerebral energy metabolism.

The purpose of this study was to demonstrate that changes in absolute $CMRO_2$ could be measured by combining NIRS and DCS. To quantify $CMRO_2$, techniques for measuring absolute CBF and cerebral blood oxygenation are required. In this study, relative blood flow changes measured by DCS were converted into units of CBF using a bolus-tracking time-resolved (TR) NIRS technique to measure baseline CBF.[17] Cerebral blood oxygenation was determined from multiwavelength TR-NIRS measurements. The accuracy of the oxygenation measurements was assessed by directly measuring blood oxygenation in the sagittal sinus. The sensitivity of the hybrid approach to changes in $CMRO_2$ was investigated by manipulating cerebral metabolism in newborn piglets by altering the anesthetics and by injecting sodium cyanide, a mitochondrial inhibitor.[18,19]

2 Methods

2.1 Animal Model

This study was approved by the Animal Use Subcommittee at Western University. Experiments were carried out on newborn

---

Address all correspondence to: K. St. Lawrence, Imaging Division, Lawson Health Research Institute, 268 Grosvenor Street, London, Ontario, N6A 4V2 Canada. Tel: +519-646-6000 ext. 65737; Fax: 519-646-6110; E-mail: kstlaw@lawsonimaging.ca

Duroc pigs (<3 days old). All surgical procedures were performed while piglets inhaled 3% to 4% isoflurane. Piglets were tracheotimized and mechanically ventilated on an oxygen/medical air mixture. Catheters were inserted into an ear vein, the left femoral artery, and superior sagittal sinus through a burr hole drilled into the skull. The ear catheter was used to inject the light-absorbing dye indocyanine green (ICG) (Sigma-Aldrich) and the different drugs used in the experiment. The femoral and sagittal sinus catheters were used to acquire blood samples to determine the oxygen saturation of arterial blood (SaO_2) and cerebral venous blood (SvO_2), respectively. The superior sagittal sinus primarily drains the cerebral cortex, which is the brain region interrogated by the optical probes.[20] The femoral line was also used to monitor heart rate, blood pressure, blood gases ($paCO_2$ and paO_2), and blood glucose. A 1- to 2-mL infusion of a 25% glucose solution was administered intravenously if glucose levels fell below 4.5 mmol/L. A heated water mattress was used to maintain rectal temperature between 37.5°C and 38.5°C throughout the experiment. After surgery, the optical probes were positioned on the scalp using a custom-made probe holder with a source-detector separation of 20 mm. A separation of 10 mm between the probes from the two optical systems ensured that they interrogated roughly the same brain region. No data were acquired for at least 30 min after surgery to ensure the piglet was physiologically stabile. Baseline conditions were identified by blood samples revealing normal $paCO_2$ and paO_2: 38–42 and 100–170 mmHg, respectively.[21]

2.2 Experimental Procedure

Five different cerebral metabolic states were induced by manipulating the anesthetics and by injecting sodium cyanide. After a change of condition, data acquisition was delayed by approximately 5 min to allow time for cerebral metabolism to stabilize. Under each condition, DCS was used to measure the blood flow index (BFI), and multiwavelength TR-NIRS was used to measure the cerebral tissue oxygen saturation (ScO_2) (see instrumentation section). Blood samples (0.3 to 0.5 mL) were drawn from the femoral artery and the sagittal sinus to determine SaO_2 and SvO_2, by hemoximetry (ABL80 Flex Co-ox, Radiometer). The DCS and TR-NIRS data were acquired in three blocks during each condition (Fig. 1). In each block, 96 TR-NIRS measurements were acquired with an integration time of 1 s, and 20 DCS measurements were acquired with an integration time of 30 s. All data sets for each condition were acquired within approximately 45 min.

Initial baseline measurements were acquired under 1.75% to 2% isoflurane mixed with a combination of medical air and oxygen to maintain normal paO_2. In addition to the standard data acquisition protocol, CBF was measured by a dynamic contrast-enhanced TR-NIR method using ICG as an intravascular contrast agent.[22] This method requires injecting an intravenous bolus of ICG (0.01 mg/kg) and measuring the time-varying concentration of ICG in arterial blood and the brain. The brain ICG concentration curve was determined by acquiring a series of TR-NIR measurements at a sampling rate of 400 ms. The arterial concentration curve was measured using a pulse dye densitometer (DDG 2001, Nihon Kohden) attached to a foot. Three successive sets of ICG data were acquired to improve the precision of the baseline CBF measurement. Successive ICG injections were separated by 10 min to allow time for ICG clearance from the previous injection. The average value of CBF was used to convert subsequent DCS BFI measurements into units of CBF.[17]

After the baseline measurements, TR-NIRS and DCS were used to measure ScO_2 and the BFI, respectively, under four conditions. First, $CMRO_2$ was increased by discontinuing isoflurane and starting an intravenous infusion of fentanyl (0.02 mg/kg/h) combined with inhalation of 70% nitrous oxide (N_2O). Second, the barbiturate pentobarbital (5 mg/kg) was injected intravenously to decrease $CMRO_2$. Cerebral energy metabolism was further reduced by switching off the fentanyl/N_2O mixture, returning the piglet to isoflurane (1.75% to 2%), and administering another 5 mg/kg of pentobarbital. For the final condition, sodium cyanide was injected intravenously at a dose of 5 mg/kg. This nonlethal dosage of cyanide is insufficient to completely inhibit mitochondrial function;[23] however, it is sufficient to reduce mitochondrial respiration.[19]

2.3 Instrumentation

2.3.1 Time-resolved NIRS system

The TR instrument for the ScO_2 measurements consisted of three picosecond diode lasers emitting at 760, 802, and 830 nm (LDH-P-C-810, PicoQuant). The output and pulse repetition rate of each laser were set to 1.4 mW and 29.3 MHz, respectively. A variable neutral density filter (NDC-50-4M, Thorlabs) was placed in front of each laser to adjust the intensity of the beam before the light was coupled into a multimode fiber (emission probe: N.A. = 0.22, $core = 400$ μm, 4.7 mm outer diameter; Fiberoptics Technology). Fibers of different lengths, forming a bundle, were used to provide time multiplexing.[24] For the ICG bolus-tracking measurements, only the 802-nm laser was used at a repetition rate of 80 MHz to optimize the signal-to-noise ratio (SNR).[25]

Reflected light from the head was collected with a 1.5-m-long multimode fiber placed 20 mm from the emission fiber bundle on the piglet's intact head. The collected photons were then sent to a Peltier-cooled photomultiplier tube (PMT)
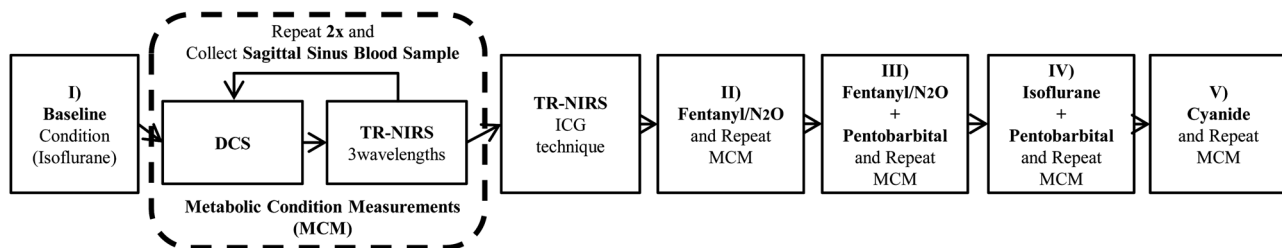
Fig. 1 Experimental protocol diagram showing the induced metabolic conditions in chronological order with the sequence of measurements acquired at each condition. The solid boxes are distinctive steps, whereas the dotted box is recurring for each induced condition numbered I–V.

(PMC-100, Becker & Hickl) coupled to a time-correlated single photon counting module (SPC-134, Becker & Hickl). Temporal point spread functions (TPSFs) were computed by synchronizing the photon detection with the laser pulse trigger provided by the driver (PDL 828, PicoQuant). Each TPSF was acquired for 1 s for the oxygenation measurements and 400 ms for the ICG bolus-tracking method. Temporal dispersion caused by the system was corrected for by measuring the instrument response function (IRF).[26] To avoid artifacts such as instrument temporal drift, the TR-NIRS system was allowed a 1.5-h warm-up delay period prior to the experiment.[25,27]

2.3.2 Diffuse correlation spectroscopy

The DCS light source was a continuous-wave laser emitting at 785 nm (DL785-100-S, CrystalLaser, Nevada) with a maximum output power of 100 mW and a coherence length >5 m. Similar to the time-resolved setup, the laser beam was first attenuated by a variable neutral density filter (NDC-50-4M, Thorlabs, New Jersey) and then coupled into an emission fiber (emission probe: N.A. = 0.22, core = 400 μm, 4.7 mm outer diameter; Fiber-optics Technology, Connecticut). Photons scattered from tissue were detected at a distance of 20 mm from the emission probe using a 4-m single-mode fiber (SMF $-$ 28e+, N.A. = 0.14, core = 125 μm, single-mode cutoff wavelength at 1260 nm). Because the detection fiber is a few-mode fiber at the laser emission wavelength, the fiber was wrapped into a 15-cm coil to attenuate the higher-order modes by converting them into non-propagating modes.[17,28,29] Photons were detected by a single photon counting module (SPCM-AQR-15-FC, PerkinElmer Canada Inc, Quebec, California). The output from the detector was sent to a correlator board (DPC-230, Becker & Hickl, Berlin, DE) to compute the normalized intensity autocorrelation function.

2.4 Data Analysis

2.4.1 Measuring cerebral oxygen saturation by TR-NIRS

Brain tissue optical properties (i.e., the absorption and reduced scattering coefficients, μ_a and μ_s', respectively) were quantified using the solution to the diffusion approximation for a semi-infinite turbid medium with extended boundary conditions.[30] The three sets of TPSFs collected at each condition were averaged together and were fitted by the theoretical model convolved with the measured IRF.[27] Initial values for μ_a, μ_s', and an amplitude scaling factor were obtained by analyzing the baseline data with a three-parameter nonlinear fitting routine.[26] The amplitude term was included in the fitting to take into account variations in laser power, detection gain, and coupling efficiency.[26,27] To improve the stability of the fitting algorithm, the TPSFs were analyzed for each metabolic condition using only μ_a as a fitting parameter; μ_s' and the amplitude scaling factor were fixed to the values retrieved from the three-parameter fit at baseline. This approach was reasonable since the metabolic changes affect only blood oxygenation and not tissue scattering properties. However, in more extreme conditions that could also alter light scattering, such as large changes in the total hemoglobin concentration,[31] μ_s' could be included as a fitting parameter. The concentrations of oxy- and deoxy-hemoglobin ([HbO$_2$] and [Hb], respectively) were derived from the measured μ_a values using the known wavelength-dependent extinction coefficients and assuming a cerebral water content of 85% for neonatal pig.[32] Cerebral oxygen saturation, ScO$_2$, was defined as

$$\text{ScO}_2 = \frac{[\text{HbO}_2]}{[\text{HbO}_2] + [\text{Hb}]}. \quad (1)$$

2.4.2 Measuring absolute CBF by TR-NIRS

The methodology underlying the TR-NIRS bolus-tracking technique for quantifying CBF, which is used extensively with imaging modalities such as magnetic resonance imaging and computed tomography,[33] assumes that the microvasculature can be modeled as a linear time-invariant system. For this application, linearity means that the contrast agent concentration in brain tissue is linearly proportional to the concentration in arterial blood, and time-invariance implies that the hemodynamic properties must remain constant during the acquisition period. Under these assumptions, the time-varying concentration of ICG in tissue, $C_t(t)$, is related to the arterial blood ICG concentration curve, $C_a(t)$, by the convolution operator

$$C_t(t) = \text{CBF}_{\text{TR}} \int_0^{\infty} C_a(t-u)R(u)\text{d}u, \quad (2)$$

where CBF$_{\text{TR}}$ denotes the CBF measurement obtained by the TR-NIRS method and $R(t)$ is the impulse residue function, which represents the fraction of ICG in the tissue at time t following an idealized unit impulse injection at $t = 0$.[34] $C_t(t)$ is determined from change in μ_a due to the passage of ICG through the cerebral microvasculature, and $C_a(t)$ was measured by the DDG as outlined in Sec. 2.2.[26] The flow-scaled impulse residue function, CBF$_{\text{TR}} \bullet R(t)$, was extracted from $C_a(t)$ and $C_t(t)$ by performing a deconvolution and its initial height equals CBF$_{\text{TR}}$, since by definition $R(0) = 1$.[22]

2.4.3 Measuring changes in CBF and CMRO$_2$ by TR-NIRS/DCS

The DCS data from each cerebral metabolic condition were analyzed by the solution to the correlation diffusion equation for a semi-infinite homogeneous medium assuming Brownian motion of scatterers.[7,8,35] The model was fitted to the normalized intensity autocorrelation function (g_2) using the μ_a and μ_s' values obtained by TR-NIRS. The fitting parameters were a scaled diffusion coefficient, which is referred to as the BFI, and a coherence factor (β).[17] The change in the BFI at a given condition relative to baseline, denoted rCBF, is given by

$$\text{rCBF} = \frac{\text{BFI}_{\text{condition}} - \text{BFI}_{\text{baseline}}}{\text{BFI}_{\text{baseline}}}. \quad (3)$$

The BFI can be converted into units of CBF (mL/100 g/ min) using the baseline CBF measurement determined by the TR-NIRS bolus-tracking method:

$$\text{CBF} = \text{CBF}_{\text{TR}}(1 + \text{rCBF}). \quad (4)$$

The CMRO$_2$ (mL O$_2$/100 g/ min) for each metabolic state was determined by conservation of mass (i.e., the Fick principle), which assumes that the amount of oxygen consumed in the tissue is equal to the arteriovenous oxygen difference:[36]

$$\text{CMRO}_2 = \text{CBF} \bullet \text{K} \bullet [\text{tHb}] \bullet (\text{SaO}_2 - \text{SvO}_2), \quad (5)$$

where SaO$_2$ and SvO$_2$ are the arterial and venous oxygen saturations, respectively; K is the oxygen-carrying capacity of

hemoglobin (1.39 mL of O_2 per g Hb);[37] and [tHb] is the total hemoglobin concentration. In these experiments, SaO_2 was measured by pulse oximetry, [tHb] was determined from the average of two baseline arterial blood samples, and CBF was determined from the calibrated DCS blood flow measurements. The remaining parameter SvO_2 was determined directly from the sagittal-sinus blood samples and also from the TR-NIRS ScO_2 measurements. Equation (5) neglects the contribution of dissolved oxygen in plasma, which is reasonable at normal paO_2 values.[38,39] For TR-NIRS, SvO_2 was determined from ScO_2 by assuming the cerebral blood volume is comprised of a known venous volume fraction (f_v), since ScO_2 represents the average cerebral blood oxygenation:

$$SvO_2 = \frac{ScO_2 - (1 - f_v)SaO_2}{f_v}. \qquad (6)$$

For this study, f_v was set to 0.75 (Refs. 40–43), and using Eq. (6), the Fick principle for the optical measurements is given by

$$CMRO_2 = \frac{CBF \bullet K \bullet [tHb]}{f_v} \bullet (SaO_2 - ScO_2). \qquad (7)$$

2.5 Statistical Analysis

Statistical analyses were conducted using SPSS 20.0 (SPSS, Chicago, Illinois). A repeated-measures analysis of variance (ANOVA) was used to identify significant differences in SvO_2 and $CMRO_2$ between metabolic conditions and between the NIRS and blood-sampling methods. Bland–Altman analysis was used to compare corresponding $CMRO_2$ measurements from the two methods.[44] Post hoc analyses were conducted to identify significant differences at each condition, with respect to baseline values, for all measured parameters. Statistical significance was defined as $p < 0.05$, and all data are presented as mean ± standard error of the mean (SEM) unless otherwise noted. In one animal, measurements were not acquired during the fentanyl/N_2O-pentobarbital condition, which was corrected for by using the missing value analysis (MVA) regression algorithm.[45]

2.6 Error Analysis

A Monte Carlo–type approach was conducted to investigate how errors in the baseline parameters would affect subsequent μ_a measurements from the one-parameter fitting routine. First, a theoretical TPSF was generated using the solution to the diffusion approximation for a semi-infinite homogeneous medium and a set of typical experimental values of the scaling amplitude, μ_a and μ_s' (8000, 0.255, and 8.62 cm^{-1}, respectively).[30] The simulated TPSF was convolved with an experimental IRF and Poisson noise added to reflect typical experimental data. The noisy TPSF was analyzed by the same nonlinear fitting routine used with the experimental data to generate best-fit estimates of the baseline parameters. Next, another noisy TPSF was generated using the initial input values, and a one-parameter fit performed to extract an estimate μ_a. In this step, the values of the amplitude factor and μ_s' were set to the estimates from three-parameter fit. The entire procedure was repeated 5000 times to generate a distribution of best-fit values for each fitting parameter.

To determine the error in $CMRO_2$ due to uncertainties in the two parameters measured under each condition (i.e., BFI and ScO_2), the SEM of each parameter was determined from the series of measurements acquired at baseline (i.e., 60 and 288 measurements for BFI and ScO_2, respectively). A repeated-measures ANOVA was used to determine the precision of the baseline CBF values measured by the TR-NIRS bolus-tracking method.

3 Results

A total of 12 piglets were studied; however, three were excluded because the sagittal sinus was inadvertently punctured during insertion of the catheter. Puncture caused blood to leak into the cerebral spinal fluid, resulting in erroneous NIRS measurements of [HbO_2] and [Hb].[18] One additional experiment was excluded due to technical errors with the TR-NIRS system, which results in incomplete TPSFs. The average physiological parameters at each metabolic condition from the eight successful experiments (three male, five female, mean weight 1.62 ± 0.09 kg, mean age 1.88 ± 0.35 days) are given in Table 1. Of all the measured parameters, only $paCO_2$ showed no significant differences between conditions. Blood pH and rectal temperature were significantly different after injecting sodium cyanide owing to the systemic effect of the drug on metabolism.

Table 1 Measured physiological parameters.

	Baseline	Fentanyl/N_2O	Fentanyl/N_2O + pentobarbital	Pentobarbital	Cyanide
Temperature (°C)	37.8 ± 0.2	37.9 ± 0.1	37.9 ± 0.2	37.4 ± 0.2	37 ± 0.2[a]
Arterial pH	7.47 ± 0.02	7.46 ± 0.02	7.46 ± 0.01	7.46 ± 0.01	7.35 ± 0.02[a]
$paCO_2$ (mmHg)	40.1 ± 0.4	39.6 ± 0.8	38.7 ± 0.7	39.8 ± 0.6	43.3 ± 2.1
paO_2 (mmHg)	124 ± 8	72 ± 5[a]	76 ± 5[a]	97 ± 8	135 ± 22
MAP (mmHg)	42 ± 2	69 ± 2[a]	82 ± 4[a]	35 ± 3	27 ± 2[a]
HR (min^{-1})	157 ± 9	241 ± 12[a]	250 ± 14[a]	165 ± 11	176 ± 7

Note: Data are averages ± SEM. $paCO_2$, partial pressure of carbon dioxide in the blood; paO_2, partial pressure of oxygen in the blood; MAP, mean arterial blood pressure; HR, heart rate.
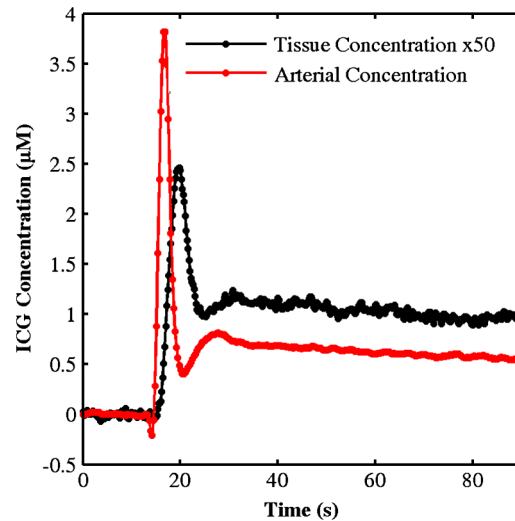[a]$p < 0.05$ compared to parameter value under baseline conditions.
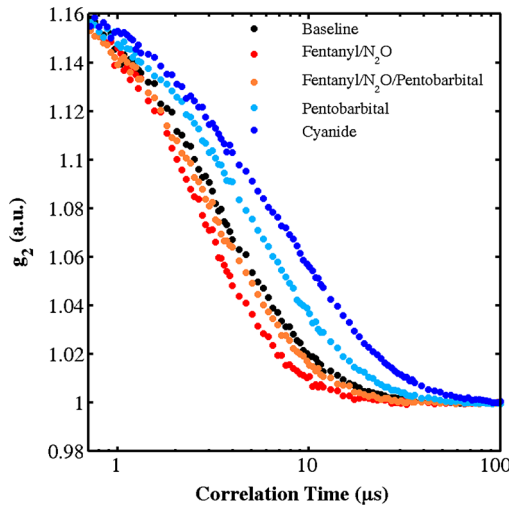
Fig. 2 DCS—condition decay curves. A sample of diffuse correlation spectroscopy (DCS) decay curves taken from an experiment collected with a sampling time of 30 s and average count rate of 441 ± 17 kHz. Each curve shown was obtained from the same piglet at a different induced metabolic condition. The steeper the decay curve, the larger the blood flow index (BFI) retrieved and ultimately the faster cerebral blood flow (CBF).

Fig. 3 ICG—arterial/tissue curves. A sample of raw data showing a tissue and an arterial curve measured during the indocyanine green (ICG) bolus tracking experiment. The black curve represents the tissue curve measured with the time-resolved near-infrared spectroscopy (TR-NIRS) technique, whereas the red curve is the arterial curve obtained from the pulse dye densitometer.

Significant differences in paO_2 were found under the two conditions involving fentanyl/N_2O, which can be explained by a reduction in the inhaled oxygen fraction during 70% N_2O inhalation. Both HR and MAP showed general changes with the different anesthetics as expected.[36] The average [tHb] measured under baseline conditions from the hemoximeter was 8.6 ± 0.8 g/dL. The tissue optical properties measured under baseline conditions at 760, 802, and 830 nm were 7.99 ± 0.47, 8.63 ± 0.59, and 8.55 ± 0.86 cm^{-1} for μ_s', respectively, and 0.251 ± 0.016, 0.240 ± 0.012, and 0.248 ± 0.009 cm^{-1} for μ_a.

Figure 2 shows a sample of DCS intensity autocorrelation curves collected from each induced metabolic condition during a single experiment. A steeper DCS decay curve is represented by a larger BFI value, indicating faster blood flow. Typical arterial and brain ICG concentration curves obtained with the DDG and TR-NIRS, respectively, are shown in Fig. 3. The derived baseline CBF value obtained from the ICG data sets was used to calibrate all subsequent BFI values obtained by DCS. The measured CBF values obtained from the dynamic contrast-enhanced technique ranged from 19 to 50 mL/100 g/min with an average of 32 ± 4 mL/100 g/min.

Significant differences were observed in all the BFI values listed in Table 2 compared to baseline, except when pentobarbital was injected while under fentanyl/N_2O anesthesia. No statistical significant differences were observed between conditions for the retrieved baseline β value of 0.157 ± 0.001, which was also in agreement with the measured value obtained by Diop et al.[17] No significant differences were observed in SaO_2 at any of the conditions. A repeated-measures ANOVA showed a significant overall effect by condition for SvO_2 [$F_{3,36} = 8.596$, Power > 0.99, $p < 0.01$], but there was no significant effect by technique [$F_{1,14} = 0.007$, $p > 0.9$]. Similarly, there was a significant effect by condition for $CMRO_2$ [$F_{3,36} = 59.707$, Power > 0.99, $p < 0.01$], but no significant effect by technique [$F_{1,14} = 0.014$, $p > 0.9$]. These results indicate that the various conditions altered cerebral energy metabolism, but there were no significant differences in the SvO_2 and $CMRO_2$

measurements between the sagittal sinus blood measurements and the DCS/NIRS method.

Figure 4 illustrates the average SvO_2 and $CMRO_2$ measurements obtained from the blood sample and DCS/TR-NIRS techniques under the different conditions. Measurements were obtained over a range from 25% to 70% for SvO_2 and from 0.3 to 4 mL O_2/100 g/min for $CMRO_2$. A Bland–Altman plot of the difference between individual $CMRO_2$ measurements from the two techniques is shown in Fig. 5. The mean difference was 0.027 mL O_2/100 g/min, with limits of agreement (i.e., 95% boundaries) of 0.861 and -0.807 mL O_2/100 g/min.

Figure 6 shows the predicted relationship between errors in the baseline optical properties to the errors in the amplitude factor as determined from the Monte Carlo simulations. The figure demonstrates that at typical experimental noise levels, μ_s' and μ_a were relatively insensitive to errors in the amplitude factor. For example, the error in either μ_s' or μ_a was only 6% in the extreme case of a 30% error in the amplitude factor. From the Monte Carlo simulations, the coefficient of variation of μ_a for the one-parameter fitting routine was 1.7%. The small magnitude of this error was also reflected in the SEM of ScO_2 (0.1%) determined from the series of baseline measurements. Similarly, the SEM of the baseline BFI was 2%. The repeat measurements of absolute CBF from the bolus tracking method indicated that this was the greatest source of error, with an estimated precision of 11.7%.

4 Discussion

The main finding of this study was that changes in absolute $CMRO_2$ could be measured by combining two near-infrared techniques: DCS and TR-NIRS. This was accomplished by combining quantitative CBF and SvO_2 measurements obtained by a previously validated DCS/TR-NIRS approach and multiwavelength TR-NIRS, respectively. The accuracy of the SvO_2 measurements was verified by comparison to direct measurements of cerebral blood oxygenation obtained from sagittal sinus blood samples. CBF, SvO_2, and $CMRO_2$ were measured

**Table 2** NIRS and blood sample measurements.

	Baseline	Fentanyl/N_2O	Fentanyl/N_2O + pentobarbital	Pentobarbital	Cyanide
BFI (cm^2/s) $\times 10^9$	61 ± 6	92 ± 10^a	62 ± 6	30 ± 5^a	28 ± 4^a
SaO_2 (%)	99.9 ± 0.1	98.8 ± 0.7	98.7 ± 0.7	99.7 ± 0.6	95.8 ± 2.3
ScO_2 (%)	69 ± 2	65 ± 3	61 ± 2	57 ± 3^a	59 ± 4
SvO_2—blood (%)	62 ± 5	55 ± 5	41 ± 5^b	42 ± 6^b	46 ± 8^b
SvO_2—NIRS (%)	58 ± 3	54 ± 4	48 ± 3^b	42 ± 4^b	46 ± 5^b
$CMRO_2$—blood (mL $O_2/100$ g/min)	1.31 ± 0.21	2.25 ± 0.25^b	2.01 ± 0.22	0.99 ± 0.18	0.76 ± 0.15^b
$CMRO_2$—NIRS (mL $O_2/100$ g/min)	1.45 ± 0.18	2.41 ± 0.32^b	1.81 ± 0.21	0.99 ± 0.17	0.80 ± 0.15^b

Note: Data are averages $\pm$ SEM. BFI, blood flow index; SaO_2, saturated arterial oxygen; ScO_2, saturated cerebral oxygen; SvO_2, saturated venous oxygen; NIRS, near-infrared spectroscopy; $CMRO_2$, cerebral metabolic rate of oxygen.
[a]$p < 0.05$ compared to parameter value under baseline conditions.
[b]$p < 0.05$ compared to parameter value under baseline conditions for both techniques combined.
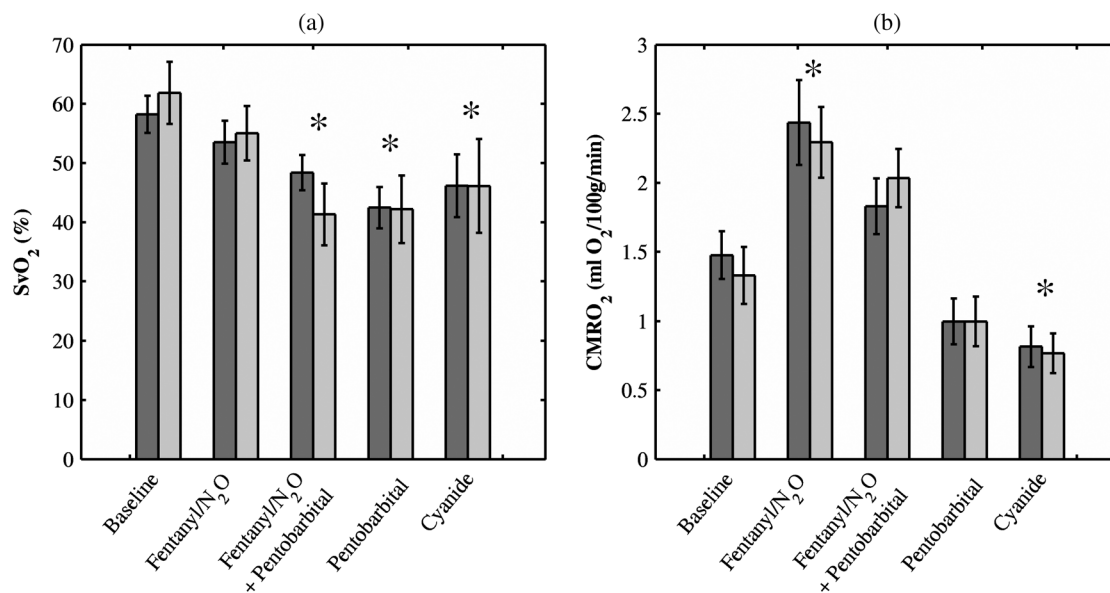

Fig. 4 Average saturated venous oxygen (SvO_2) and cerebral metabolic rate of oxygen ($CMRO_2$) values at each induced condition comparing both techniques. The darker gray bars represent the NIRS technique, the lighter gray bars represent the blood oxygen sample method, and the error bars are standard error of the mean. *$p < 0.05$ compared to the parameter value under baseline conditions for both techniques combined.

over a metabolic range from approximately 0.3 to 4 mL $O_2/100$ g/min with no evidence of any level-dependent bias in either the SvO_2 or $CMRO_2$ measurements (Figs. 4 and 5). DCS and NIRS have been combined previously to measure relative changes in $CMRO_2$;[9–12,46] however, this is the first study to use this combination to quantify $CMRO_2$. The success of this combined optical approach ultimately depends on the accuracy of the underlying CBF and ScO_2 measurements. A number of studies have demonstrated the ability of DCS to track relative CBF.[17,47–50] In particular, Zhou et al.[49] reported a strong correlation between changes in CBF measured by DCS and those measured by fluorescent microspheres in newborn piglets. Similarly, we previously reported a strong correlation between CBF measurements obtained by the bolus-tracking TR-NIRS technique and the BFI determined from DCS ($R_2 = 0.93$).[17]

In our previous study, a single pulsed laser was used to measure the absorption changes caused by the flow of ICG through brain tissue.[22] Determining [HbO_2] and [Hb], and thereby ScO_2, requires measuring the tissue optical properties at multiple wavelengths. For this purpose, the TR system was expanded to three pulsed lasers, and time multiplexing was used to acquire the corresponding three TPSFs within the same time window.[24] The disadvantage of this approach is a lower count rate per channel due to the reduced pulse repetition rate (29.3 compared to 80 MHz); however, for steady-state oxygenation measurements, this was not a concern, as the SNR can be improved by increasing the integration time. To quantify the wavelength-dependent μ_a and μ_s' values, the IRF was measured for each laser at similar count rates to those obtained experimentally. Temporal drift and variations in the laser pulse width (i.e., jitter) are potential sources of error when measuring tissue optical properties by TR-NIRS.[27] To minimize the former, every experiment was preceded by a 1.5-h delay to allow sufficient time for the TR-NIRS system to stabilize to avoid instrument drift during the course of
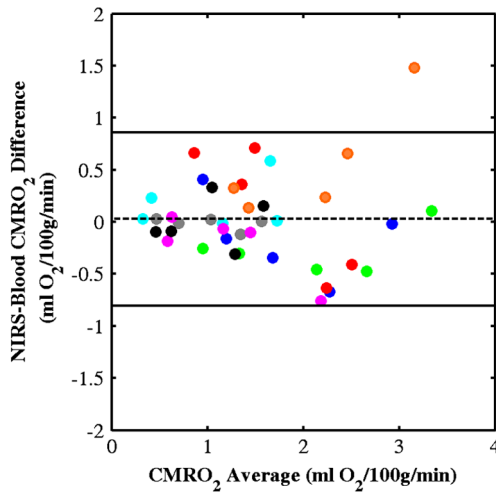
Fig. 5 A Bland–Altman plot demonstrating the difference between NIRS and blood oxygen sample $CMRO_2$ measurements plotted against the average. Each color represents a different piglet. The dotted line represents the average difference between the two techniques, 0.027 mL $O_2/100$ g/ min. The solid lines are the bias lines which represent the region boundaries for which 95% of the differences that lie within, 0.027 ± 0.834 mL $O_2/100$ g/ min.
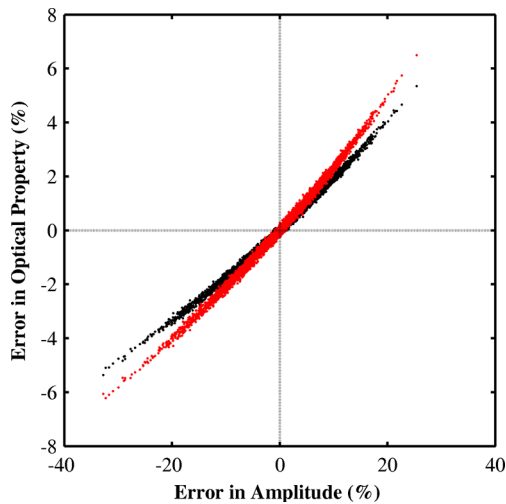
Fig. 6 An error analysis comparing the effects of noisy experimental data on a three-parameter fit (μ_a, μ_s', and amplitude factor) from the diffusion approximation. Black represents μ_a and red represents μ_s', while each data point represents the error in optical properties corresponding to the error in the amplitude factor from the three parameter fit. The generated noise for 5000 simulated temporal point spread functions (TPSFs) had an average variance of 16.41 ± 0.05.

an experiment.[25] The results displayed in Fig. 6 indicate that the baseline μ_a and μ_s' values could be determined with reasonable accuracy even if there were large fluctuations in the amplitude factor, such as due to jitter. A possible improvement to the system would be to correct for both drift and jitter by acquiring reference data throughout the experiment.[51]

The precision of $CMRO_2$ will depend on the uncertainties in the baseline optical properties, CBF and ScO_2. The Monte Carlo simulations demonstrated that the uncertainties in the optical properties were small for noise levels typical of the experimental TPSFs and had little effect on subsequent μ_a values determined from the one-parameter fitting routine. These predictions were

in good agreement with the SEM of ScO_2 (0.1%) determined from the series of TPSFs acquired during the 5-min baseline period. Errors in CBF determined by the calibrated DCS approach will depend on the precision of both the baseline CBF determined by the bolus-tracking method and the relative BFI obtained by DCS. From repeat bolus injections at baseline, the precision of the former was estimated to be 11.7%, which is similar to the value determined previously (9.7%) with a continuous-wave NIRS system.[22] In these experiments, the SEM of the BFI was <2% due to the large number of acquisitions obtained in each condition. A variability of <5% would still have been achieved if the acquisition time had been reduced to 5 min (i.e., 10 measurements). Maintaining the same precision at shorter acquisitions would require increasing the number of detectors,[28,47] as only a single SPCM was used to acquire the DCS data in these experiments. In addition to the uncertainties in the measurements parameters, the accuracy of the $CMRO_2$ measurements will depend on the assumed value of the cerebral venous blood volume fraction (f_v). The need to assume a value is a common limitation with $CMRO_2$ measurements obtained by NIRS and positron emission tomography.[18,39,52] The good agreement between the NIRS $CMRO_2$ measurements and the values derived from sagittal-sinus blood samples (Fig. 5) indicate that the assumed value of 75% is reasonable. However, any variation in f_v across animals or subjects will clearly reduce the accuracy of the measurements. It may be possible to circumvent this potential source of error by using NIRS spiroximetry to measure venous oxygen saturation.[53]

The retrieved μ_s' values at baseline were similar to those of Diop et al.[17] and Ijichi et al.[43] However, the average μ_a at 802 nm was greater than the values given in the two previous studies: 0.2 ± 0.009 cm^{-1} (Ref. 17) and 0.189 ± 0.005 (Ref. 43). The cause of this difference is uncertain; however, the average ScO_2 value (69% $\pm$ 2%) was similar to baseline values previously reported in piglets.[54–57] In addition, the SvO_2 values determined from the absorption changes at the different metabolic conditions ranging from 25% to 70% were in good agreement with the corresponding SvO_2 values measured directly from sagittal sinus blood samples (Table 2, Fig. 4). Both sets displayed the same trend in venous oxygenation, as cerebral metabolism was initially increased under fentanyl/ N_2O anesthesia and subsequently decreased with successive injections of pentobarbital.

The overall agreement between $CMRO_2$ measurements derived from TR-NIRS and sagittal sinus SvO_2 values is similar to our previous validation study, which was conducted using newborn piglets but involved a broadband CW-NIRS system.[18] In that study, the mean difference between the two techniques was 0.006 mL $O_2/100$ g/ min, and the 95% confidence interval was ±0.74 mL $O_2/100$ g/ min. The latter is slightly smaller than the boundaries shown in Fig. 5. However, this difference can be explained by the outlier that had an average $CMRO_2$ difference greater than the 95% confidence interval. Removing this point reduced the range to ±0.704 mL $O_2/100$ g/ min, in excellent agreement with the previous results. It is interesting that the overall trends reported in the two studies were in good agreement considering the different approaches used to quantify cerebral blood oxygenation. The CW-NIRS spectral data from the previous study were characterized by second derivative spectroscopy, which can only estimate [Hb] and not [HbO$_2$], since the latter has no definitive features in the derivative spectrum.[58] Consequently, $CMRO_2$ was determined by normalizing [Hb] by

the cerebral blood volume. This step is not required for TR-NIRS, since both [Hb] and [HbO$_2$] are determined from the measured optical properties. A further advantage to directly measuring μ_a and μ_s' by TR-NIRS is that these values can also be used in the analysis of DCS data rather than assuming known values. Another advantage with TR-NIRS is its superior depth sensitivity, which could prove useful when adapting these optical technologies to measuring CBF and CMRO$_2$ in adult patients.[59,60]

Although the two studies demonstrate similar agreements between the NIRS and sagittal sinus CMRO$_2$ measurements, there was a large difference in the initial baseline CMRO$_2$ values: 1.48 ± 0.17 mL O$_2$/100 g/min in the current study and 2.60 ± 0.28 mL O$_2$/100 g/min from Tichauer et al.[18] One possible explanation is the difference in baseline anesthetics in the two studies. Baseline measurements in the current study were acquired using a higher concentration of isoflurane (1.75% to 2% compared to 1.5%), which will reduce cerebral energy metabolism. Another contributing factor could be the difference in CBF measurements from CW- and TR-NIRS techniques. Previously, we have demonstrated that the CBF values from TR-NIRS underestimated the CW-NIRS values, although the reason for this difference was unclear.[26] Adjusting the current CMRO$_2$ values for this difference would increase the mean baseline value to 2.00 ± 0.22 mL O$_2$/100 g/min, which is still below our previous results. Most likely, the overall difference between the two studies is a combination of both factors.

In addition to the different anesthetics, measurements were also conducted after administering sodium cyanide. This drug was used to alter cerebral oxidative metabolism by an alternative means, namely, the inhibition of mitochondrial cytochrome oxidase. Overall, the agreement between the DCS/TR-NIRS and sagittal sinus CMRO$_2$ values under this condition was similar to that observed under the different anesthetics. However, the metabolic effect of cyanide was smaller than expected based on a previous study involving newborn piglets.[19] This muted effect is likely a result of injecting the sodium cyanide while the animals were under the deepest anesthetic (pentobarbital plus isoflurane). Nevertheless, cyanide did cause a small reduction in CMRO$_2$, which was observable by both techniques.

A potential limitation with the current study is that the CBF measurements obtained by the calibrated DCS technique were used to convert both the sagittal-sinus and NIRS venous oxygenation measurements into CMRO$_2$. Consequently, any systemic error in the optical CBF measurements would not be observed in this study. We previously demonstrated a very strong correlation between relative flow changes measured by DCS and CBF values measured by TR-NIRS with a slope from the linear regression of 1.05 (Ref. 17). This comparison was conducted over a range of CBF values from 17 to 90 mL/100 g/min, which is very similar to the range observed in the current study. However, more validation studies would be required if the combined DCS/TR-NIRS approach were used to measure CMRO$_2$ under pathological conditions such as during ischemia or severe hypoxia that could result in greater changes in either CBF or SvO$_2$.[16,43]

In summary, this study demonstrated that the combination of DCS and TR-NIRS can be used to measure CMRO$_2$ as verified by the comparison to CMRO$_2$ values derived from cerebral venous blood samples. Experiments were conducted using piglets because they are similar in size to human newborns and, therefore, the DCS/TR-NIRS system could be used in clinical studies. Adapting this approach to the neonatal intensive care unit will require synchronizing the two optical systems to provide truly continuous CBF and CMRO$_2$ measurements. Extending this approach to adult patients represents a significant challenge, as it requires depth-resolved techniques, such as the use of multilayered modeling approaches, to accurately measure CBF, cerebral oxygenation, and BFI.[61–63] Incorporating sensitivity functions for the different tissue layers into the analysis of bolus tracking data has been shown to improve the accuracy of CBF measurements in animal models; however, clinical studies will require validating this approach in human subjects.[60,64]

References

1. R. Behrman, "Institute of Medicine (US) Committee on understanding premature birth and assuring healthy outcomes," *Preterm Birth: Causes, Consequences, and Prevention*, pp. 1–4, National Academies Press, Washington, DC (2006).
2. J. Volpe, "Brain injury in the premature infant: is it preventable?," *Pediatr. Res.* **27**, S28–S33 (1990).
3. J. S. Soul et al., "Fluctuating pressure-passivity is common in the cerebral circulation of sick premature infants," *Pediatr. Res.* **61**, 467–473 (2007).
4. H. O'Leary et al., "Elevated cerebral pressure passivity is associated with prematurity-related intracranial hemorrhage," *Pediatrics* **124**(1), 302–309 (2009).
5. F. Y. Wong, T. S. Leung, T. Austin, M. Wilkinson, J. H. Meek, J. S. Wyatt, and A. M. Walker, "Impaired autoregulation in preterm infants identified by using spatially resolved spectroscopy," *Pediatrics* **121**(3), e604–e611 (2008).
6. J. Cooper et al., "Continuous monitoring of absolute cerebral blood flow by near-infrared spectroscopy during global and focal temporary vessel occlusion," *J. Appl. Physiol.* **110**(6), 1691–1698 (2011).
7. D. Boas and A. G. Yodh, "Spatially varying dynamical properties of turbid media probed with diffusing temporal light correlation," *J. Opt. Soc. Am. A* **14**(1), 192 (1997).
8. C. Cheung et al., "*In vivo* cerebrovascular measurement combining diffuse near-infrared absorption and correlation spectroscopies," *Phys. Med. Biol.* **46**(8), 2053–2065 (2001).
9. T. Durduran et al., "Optical measurement of cerebral hemodynamics and oxygen metabolism in neonates with congenital heart defects," *J. Biomed. Opt.* **15**(3), 037004 (2010).
10. N. Roche-Labarbe et al., "Noninvasive optical measures of CBV, StO(2), CBF index, and rCMRO(2) in human premature neonates' brains in the first six weeks of life," *Hum. Brain Mapp.* **31**(3), 341–352 (2010).
11. N. Roche-Labarbe et al., "Near-infrared spectroscopy assessment of cerebral oxygen metabolism in the developing premature brain," *J. Cereb. Blood Flow Metab.* **32**, 481–488 (2012).
12. T. Durduran et al., "Diffuse optical measurement of blood flow, blood oxygenation, and metabolism in a human brain during sensorimotor cortex activation," *Opt. Lett.* **29**(15), 1766–1768 (2004).
13. W. Powers et al., "Cerebral blood flow and cerebral metabolic rate of oxygen requirements for cerebral function and viability in humans," *J. Cereb. Blood Flow Metab.* **5**, 600–608 (1985).
14. D. Boas and M. A. Franceschini, "Haemoglobin oxygen saturation as a biomarker: the problem and a solution," *Philos. Trans. A Math. Phys. Eng. Sci.* **369**, 4407–4424 (2011).
15. K. M. Tichauer et al., "Cerebral metabolic rate of oxygen and amplitude-integrated electroencephalography during early reperfusion after hypoxia-ischemia in piglets," *J. Appl. Physiol.* **106**(5), 1506–1512 (2009).

16. K. M. Tichauer, D. W. Brown, J. Hadway, T.-Y. Lee, and K. St. Lawrence, "Near-infrared spectroscopy measurements of cerebral blood flow and oxygen consumption following hypoxia-ischemia in newborn piglets," *J. Appl. Physiol.* **100**(3), 850–857 (2006).

17. M. Diop et al., "Calibration of diffuse correlation spectroscopy with a time-resolved near-infrared technique to yield absolute cerebral blood flow measurements," *Biomed. Opt. Exp.* **2**(7), 2068–2081 (2011).

18. K. M. Tichauer, J. Hadway, T.-Y. Lee, and K. St. Lawrence, "Measurement of cerebral oxidative metabolism with near-infrared spectroscopy: a validation study," *J. Cereb. Blood Flow Metab.* **26**, 722–730 (2006).

19. C. Cooper et al., "Use of mitochondrial inhibitors to demonstrate that cytochrome oxidase near-infrared spectroscopy can measure mitochondrial dysfunction noninvasively in the brain," *J. Cereb. Blood Flow Metab.* **19**, 27–38 (1999).

20. O. Scremin, R. R. Sonnenschein, and E. H. Rubinstein, "Cerebrovascular anatomy and blood flow measurements in the rabbit," *J. Cereb. Blood Flow Metab.* **2**, 55–66 (1982).

21. M. Reivich, "Arterial PCO2 and cerebral hemodynamics," *Am. J. Physiol. Legacy* **206**(1), 25–35 (1964).

22. D. W. Brown et al., "Quantitative near infrared spectroscopy measurement of cerebral hemodynamics in newborn piglets," *Pediatr. Res.* **51**, 564–570 (2002).

23. T. Sakamoto et al., "Utility and limitations of near-infrared spectroscopy during cardiopulmonary bypass in a piglet model," *Pediatr. Res.* **49**, 770–776 (2001).

24. D. Contini et al., "Multi-channel time-resolved system for functional near infrared spectroscopy," *Opt. Exp.* **14**(12), 5418–5432 (2006).

25. M. Diop et al., "Time-resolved near-infrared technique for bedside monitoring of absolute cerebral blood flow," *Proc. SPIE* **7555**, 75550Z-1–75550Z-9 (2010).

26. M. Diop et al., "Comparison of time-resolved and continuous-wave near-infrared techniques for measuring cerebral blood flow in piglets," *J. Biomed. Opt.* **15**(5), 057004 (2010).

27. V. Ntziachristos and B. Chance, "Accuracy limits in the determination of absolute optical properties using time-resolved NIR spectroscopy," *Med. Phys.* **28**, 1115 (2001).

28. G. Dietsche et al., "Fiber-based multispeckle detection for time-resolved diffusing-wave spectroscopy: characterization and application to blood flow detection in deep tissue," *Appl. Opt.* **46**(35), 8506–8514 (2007).

29. T. Gisler et al., "Mode-selective dynamic light scattering: theory versus experimental realization," *Appl. Opt.* **34**(18), 3546–3553 (1995).

30. A. Kienle and M. Patterson, "Improved solutions of the steady-state and the time-resolved diffusion equations for reflectance from a semi-infinite turbid medium," *J. Opt. Soc. Am. A* **14**(1), 246–254, (1997).

31. L. A. Paunescu et al., "*In vitro* correlation between reduced scattering coefficient and hemoglobin concentration of human blood determined by near-infrared spectroscopy," *Proc. SPIE* 319–326 (2001).

32. B. A. Holland et al., "MRI of normal brain maturation," *Am. J. Neuroradiol.* **7**(2), 201–208 (1986).

33. M. Wintermark et al., "Comparative overview of brain perfusion imaging techniques," *Stroke* **36**, e83–99 (2005).

34. K. L. Zierler, "Equations for measuring blood flow by external monitoring of radioisotopes," *Circ. Res.* **16**, 309–321 (1965).

35. D. Boas, L. Campbell, and A. G. Yodh, "Scattering and imaging with diffusing temporal field correlations," *Phys. Rev. Lett.* **75**, 1855–1858 (1995).

36. B. Siesjo, "Brain energy metabolism and catecholaminergic activity in hypoxia, hypercapnia and ischemia," *J. Neural. Transm. Suppl.* **14**, 17–22 (1978).

37. E. D. Dominguez de Villota et al., "Equality of the *in vivo* and *in vitro* oxygen-binding capacity of haemoglobin in patients with severe respiratory disease," *Br. J. Anaesth.* **53**(12), 1325–1328 (1981).

38. D. W. Brown, J. Hadway, and T.-Y. Lee, "Near-infrared spectroscopy measurement of oxygen extraction fraction and cerebral metabolic rate of oxygen in newborn piglets," *Pediatr. Res.* **54**, 861–867 (2003).

39. C. E. Elwell et al., "Measurement of CMRO2 in neonates undergoing intensive care using near infrared spectroscopy," *Adv. Exp. Med. Biol.* **566**, 263–268 (2005).

40. G. Mchedlishvili, *Arterial Behavior and Blood Circulation in the Brain*, J. Bevan, Ed., p. 56, Consultants Bureau, New York (1986).

41. H. H. M. Watzman et al., "Arterial and venous contributions to near-infrared cerebral oximetry," *Anesthesiology* **93**(2), 947 (2000).

42. N. Brun, A. Moen, and K. Borch, "Near-infrared monitoring of cerebral tissue oxygen saturation and blood volume in newborn piglets," *Am. J. Physiol.* **273**(2), H682–H686 (1997).

43. S. Ijichi et al., "Quantification of cerebral hemoglobin as a function of oxygenation using near-infrared time-resolved spectroscopy in a piglet model of hypoxia," *J. Biomed. Opt.* **10**(2), 024026 (2005).

44. D. Altman and J. Bland, "Measurement in medicine: the analysis of method comparison studies," *J. Roy. Stat. Soc. Series D (The Statistician)* **32**(3), 307–317 (1983).

45. J. W. Graham, "Missing data analysis: making it work in the real world," *Ann. Rev. Psychol.* **60**, 549–576 (2009).

46. P. Zirak et al., "Effects of acetazolamide on the micro- and macro-vascular cerebral hemodynamics: a diffuse optical and transcranial doppler ultrasound study," *Biomed. Opt. Exp.* **1**(5), 1443–1459 (2010).

47. E. M. Buckley et al., "Cerebral hemodynamics in preterm infants during positional intervention measured with diffuse correlation spectroscopy and transcranial Doppler ultrasound," *Opt. Exp.* **17**(15), 12571–12581 (2009).

48. S. A. Carp et al., "Validation of diffuse correlation spectroscopy measurements of rodent cerebral blood flow with simultaneous arterial spin labeling MRI; towards MRI-optical continuous cerebral metabolic monitoring," *Biomed. Opt. Exp.* **1**(2), 553–565 (2010).

49. C. Zhou et al., "Diffuse optical monitoring of hemodynamic changes in piglet brain with closed head injury," *J. Biomed. Opt.* **14**(3), 034015 (2009).

50. M. N. Kim et al., "Noninvasive measurement of cerebral blood flow and blood oxygenation using near-infrared and diffuse correlation spectroscopies in critically brain-injured adults," *Neurocrit. Care* **12**(2), 173–180 (2010).

51. K. M. Tichauer et al., "Imaging workflow and calibration for CT-guided time-domain fluorescence tomography," *Biomed. Opt. Exp.* **2**(11), 3021–3036 (2011).

52. M. Mintun et al., "Brain oxygen utilization measured with O-15 radiotracers and positron emission tomography," *J. Nucl. Med.* **25**(2), 177–187 (1984).

53. M. A. Franceschini et al., "Near-infrared spiroximetry: noninvasive measurements of venous saturation in piglets and human subjects," *J. Appl. Physiol.* **92**(1), 372–384 (2002).

54. T. Kusaka et al., "Quantification of cerebral oxygenation by full-spectrum near-infrared spectroscopy using a two-point method," *Compar. Biochem. Physiol. A Mol. Integ. Physiol.* **132**(1), 121–132 (2002).

55. S. Fantini et al., "Non-invasive optical monitoring of the newborn piglet brain using continuous-wave and frequency-domain spectroscopy," *Phys. Med. Biol.* **44**(6), 1543–1563 (1999).

56. R. Springett et al., "Oxygen dependency and precision of cytochrome oxidase signal from full spectral NIRS of the piglet brain," *Am. J. Physiol. Heart Circ. Physiol.* **279**(5), H2202–H2209 (2000).

57. C. D. Kurth et al., "Cerebral oxygen saturation-time threshold for hypoxic-ischemic injury in piglets," *Anesth. Analges.* **108**, 1268–1277 (2009).

58. S. Matcher, M. Cope, and D. T. Delpy, "Use of the water absorption spectrum to quantify tissue chromophore concentration changes in near-infrared spectroscopy," *Phys. Med. Biol.* **39**(1), 177–196 (1994).

59. A. Liebert et al., "Time-resolved multidistance near-infrared spectroscopy of the adult head: intracerebral and extracerebral absorption changes from moments of distribution of times of flight of photons," *Appl. Opt.* **43**(15), 3037–3047 (2004).

60. J. T. Elliott et al., "Quantitative measurement of cerebral blood flow in a juvenile porcine model by depth-resolved near-infrared spectroscopy," *J. Biomed. Opt.* **15**(3), 037014 (2010).

61. L. Gagnon et al., "Investigation of diffuse correlation spectroscopy in multi-layered media including the human head," *Opt. Express* **16**(20), 15514–15530, (2008).

62. F. Jaillon et al., "Diffusing-wave spectroscopy from head-like tissue phantoms: influence of a non-scattering layer," *Opt. Express* **14**(22), 10181–10194 (2006).

63. H. Wabnitz et al., "Time-resolved near-infrared spectroscopy and imaging of the adult human brain," *Adv. Exp. Med. Biol.* **662**, E. Takahashi and D. F. Bruley, Eds., pp. 143–148, Springer US, Boston, MA (2010).

64. J. T. Elliott et al., "Model-independent dynamic constraint to improve the optical reconstruction of regional kinetic parameters," *Opt. Lett.* **37**(13), 2571–2573 (2012).